Editors' Suggestion

Microwave Engineering of Programmable *XXZ* Hamiltonians in Arrays of Rydberg Atoms

P. Scholl,[1,†] H. J. Williams,[1,†] G. Bornet,[1,†] F. Wallner,[1,‡] D. Barredo,[1,§] L. Henriet,[2] A. Signoles,[2] C. Hainaut,[3] T. Franz,[3] S. Geier,[3] A. Tebben,[3] A. Salzinger,[3] G. Zürn,[3] T. Lahaye,[1] M. Weidemüller,[3] and A. Browaeys[1,*]

[1] *Université Paris-Saclay, Institut d'Optique Graduate School, CNRS, Laboratoire Charles Fabry, Palaiseau Cedex 91127, France*

[2] *Pasqal, 2 avenue Augustin Fresnel, Palaiseau 91120, France*

[3] *Physikalisches Institut, Universität Heidelberg, Im Neuenheimer Feld 226, Heidelberg 69120, Germany*

(Received 30 July 2021; revised 9 February 2022; accepted 25 February 2022; published 5 April 2022)

We use the resonant dipole-dipole interaction between Rydberg atoms and a periodic external microwave field to engineer *XXZ* spin Hamiltonians with tunable anisotropies. The atoms are placed in one-dimensional (1D) and two-dimensional (2D) arrays of optical tweezers. As illustrations, we apply this engineering to two iconic situations in spin physics: the Heisenberg model in square arrays and spin transport in 1D. We first benchmark the Hamiltonian engineering for two atoms and then demonstrate the freezing of the magnetization on an initially magnetized 2D array. Finally, we explore the dynamics of 1D domain-wall systems with both periodic and open boundary conditions. We systematically compare our data with numerical simulations and assess the residual limitations of the technique as well as routes for improvement. The geometrical versatility of the platform, combined with the flexibility of the simulated Hamiltonians, opens up exciting prospects in the fields of quantum simulation, quantum information processing, and quantum sensing.

DOI: 10.1103/PRXQuantum.3.020303

I. INTRODUCTION

Quantum simulation using synthetic quantum systems is now becoming a fruitful approach to explore open questions in many-body physics [1]. Experimental platforms that have been used for quantum simulation so far include ions [2,3], molecules [4,5], atoms [6,7], and quantum circuits [8,9]. These systems naturally implement particular instances of many-body Hamiltonians, such as those describing the interactions between spins or the Bose- and Fermi-Hubbard Hamiltonians [7]. Each platform already features a high degree of programmability, with the possibility of tuning many of the parameters of the simulated Hamiltonians. In the quest for fully programmable quantum simulators, one would like to extend the capabilities to simulate Hamiltonians beyond those that are naturally implemented. In this spirit, applying a periodic drive to a system allows for the engineering of a broader class of Hamiltonians, where additional parameters can be modified at will. This Floquet-engineering technique [10], initially introduced in the context of NMR [11,12], has been used for digital quantum simulation [13] and to explore new physical phenomena such as dynamical phase transitions [14], Floquet prethermalization [15,16], novel phases of matter [17], and topological configurations [18–23].

Among the platforms being developed, the one based on Rydberg atoms held in arrays of optical tweezers is a promising candidate for quantum simulation [24] and computation [25,26]. Recent works have demonstrated its potential through the implementation of different spin models. First, an ensemble of Rydberg atoms coupled by the van der Waals interaction naturally realizes the quantum transverse-field Ising model. Using this fact, arrays containing up to hundreds of atoms have been used to prepare antiferromagnetic order in two dimensions (2D) [27–29] or three dimensions (3D) [30], study exotic phases

*antoine.browaeys@institutoptique.fr

†These authors contributed equally to this work.

‡Also at Department of Physics, Technical University of Munich, James-Franck-Strasse 1, 85748 Garching, Germany.

§Also at Nanomaterials and Nanotechnology Research Center (CINN-CSIC), Universidad de Oviedo (UO), Principado de Asturias, 33940 El Entrego, Spain.

and quantum phase transitions [31,32], and observe the first evidence of a spin liquid [33]. Second, the resonant dipole-dipole interaction between Rydberg atoms in states with opposite parity implements an *XXZ* spin Hamiltonian, which has been used to realize a density-dependent Peierls phase [34] and to prepare a symmetry-protected topological phase in one dimension (1D) [35]. Finally, the dipolar interaction for two Rydberg atoms in states with the same parity leads to a *XXZ* spin Hamiltonian with anisotropy *fixed* by the choice of the principal quantum number [36], as demonstrated in a gas of cold atoms [37]. Circular Rydberg atoms also offer the promise of realizing the *XXZ* model with anisotropy tunable by external electric and magnetic fields [38].

Besides these naturally implemented models, more general spin models, such as *XYZ* models, which can feature SU(2), U(1), or even the absence of unitary symmetries, are also of general interest to study ground-state [39] and out-of-equilibrium many-body physics [40]. In this context, transport properties of spin excitations are actively studied, both experimentally and theoretically (see, e.g., Refs. [41–45]). For 1D systems, the behavior is known to be highly dependent on the parameters of the Hamiltonians [46]. Several experimental methods, involving the relaxation of spin-spiral states [47,48] or the melting of initially prepared domain walls [49,50], enable the extraction of global transport behaviors ranging from ballistic to localized ones as a function of the Hamiltonian parameters. Furthermore, the experimental development of single-atom resolution techniques gives access to the exploration of transport properties through correlation functions, as demonstrated with trapped ions [51–53] or ultracold atoms in optical lattices [54].

Programmable *XXZ* Hamiltonians have recently been demonstrated on a periodically driven Rydberg gas where the atoms are coupled by the resonant dipole-dipole interaction [55]. This technique offers the opportunity to arbitrarily and dynamically tune the anisotropy of the applied Hamiltonian. However, the use of a gas in Ref. [55] prevented the direct observation of the underlying coherent dynamics. Here, we extend this demonstration to the case of *ordered* arrays of Rydberg atoms with individual addressing and measurement capabilities. The versatility and control of the platform allows us to implement the *XXZ* Hamiltonian in several situations, ranging from 1D with open or periodic boundary conditions to 2D geometries. This enables us to explore *coherent* spin transport in a few-body system through the investigation of domain-wall melting experiments.

II. MICROWAVE ENGINEERING OF *XXZ* HAMILTONIANS

In this section, we apply the average Hamiltonian theory to the specific case of Rydberg atoms and briefly show how to engineer the *XXZ* spin model with tunable parameters. We closely follow the approach developed in Ref. [12,55].

We consider an array of Rydberg atoms, each described as a two-level system with states of opposite parity mapped onto pseudospin states: $|nS\rangle = |\downarrow\rangle$ and $|nP\rangle = |\uparrow\rangle$. The resonant dipole-dipole interaction couples the atoms, leading to the *XXZ* Hamiltonian:

$$H_{XX} = \frac{1}{2}\sum_{i\neq j} J_{ij}\,(\sigma_i^x\sigma_j^x + \sigma_i^y\sigma_j^y). \tag{1}$$

Here, $J_{ij} = C_3(1-3\cos^2\theta_{ij})/(2r_{ij}^3)$, where r_{ij} is the distance between atoms i and j, θ_{ij} gives their angle compared to the quantization axis, and $\sigma_i^x = |\uparrow\rangle\langle\downarrow|_i + |\downarrow\rangle\langle\uparrow|_i$ and $\sigma_i^y = i(|\uparrow\rangle\langle\downarrow|_i - |\downarrow\rangle\langle\uparrow|_i)$ are the Pauli matrices for atom i. With the addition of a resonant microwave field to couple the $|\downarrow\rangle$ and $|\uparrow\rangle$ states, the Hamiltonian becomes, in the rotating-wave approximation,

$$H_{\text{driven}} = H_{XX} + \frac{\hbar\Omega(t)}{2}\sum_i \cos\phi(t)\sigma_i^x + \sin\phi(t)\sigma_i^y, \tag{2}$$

where $\Omega(t)$ and $\phi(t)$ are the Rabi frequency and phase of the microwave field, respectively. We use a sequence $(X, -Y, Y, -X)$ of four $\pi/2$ Gaussian pulses, with constant phases $\phi = (0, -\pi/2, \pi/2, \pi)$ separated by durations $\tau_{1,2}$ and $2\tau_3$, shown in Fig. 1(a). The time average of H_{driven} over a sequence leads to the time-independent Hamiltonian H_{av}:

$$H_{\text{av}} = \frac{1}{2}\sum_{i\neq j}\frac{2J_{ij}}{t_c}[(\tau_1+\tau_2)\sigma_i^x\sigma_j^x + (\tau_1+\tau_3)\sigma_i^y\sigma_j^y + (\tau_2+\tau_3)\sigma_i^z\sigma_j^z], \tag{3}$$

where $t_c = 2(\tau_1+\tau_2+\tau_3)$ is the total duration of the sequence. The dynamics of the system is governed in good approximation by H_{av} when the duration of each pulse is negligible with respect to t_c. Moreover, t_c needs to be much shorter than the interaction time scales set by the averaged interaction energy $J_m = 1/N\sum_{i\neq j} J_{ij}$, where N is the total number of spins. This leads to the requirement $J_m t_c \ll 2\pi$. As the number of nearest neighbors, and hence J_m, depends on the geometry of the array, t_c must be adapted accordingly. Equation (3) has the form of an *XYZ* Hamiltonian, the coefficients of which are tunable by simply varying the delays between the pulses. In this work, we restrict ourselves to the case of the *XXZ* Hamiltonian, which conserves the number of spin excitations:

$$H_{XXZ} = \frac{1}{2}\sum_{i\neq j} J_{ij}^x(\sigma_i^x\sigma_j^x + \sigma_i^y\sigma_j^y) + J_{ij}^z\sigma_i^z\sigma_j^z, \tag{4}$$

where $J_{ij}^x = J_{ij}^y = 2J_{ij}(\tau_1+\tau_2)/t_c$ and $J_{ij}^z = 4J_{ij}\tau_2/t_c$, with $\tau_2 = \tau_3$. The anisotropy of the Hamiltonian

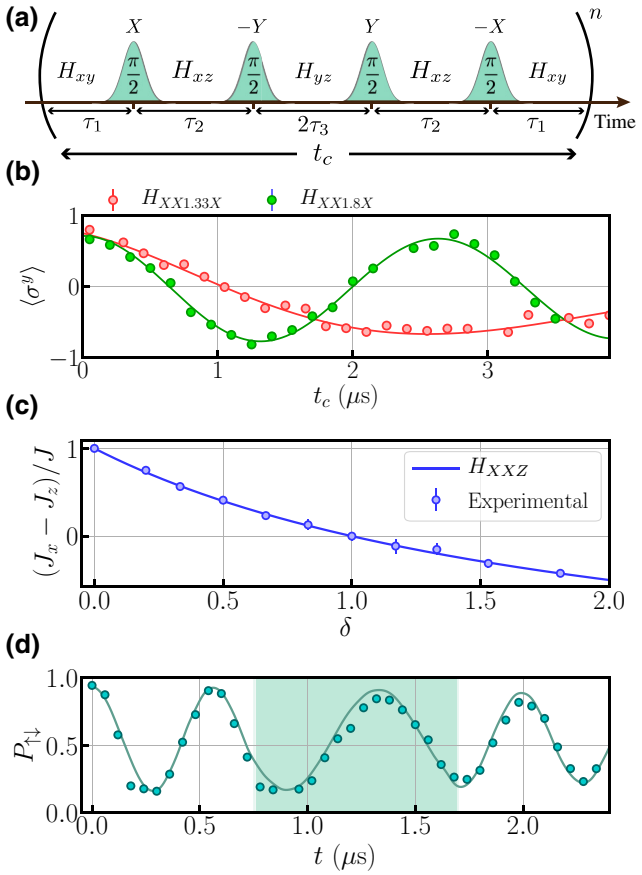

FIG. 1. The implementation of *XXZ* Hamiltonians with two atoms. (a) The microwave sequence consisting of four $\pi/2$ Gaussian pulses driving rotations around the X, $-Y$, Y, and $-X$ axes. (b) The evolution of the y magnetization under H_{driven} after initialization in $|{\rightarrow}{\rightarrow}\rangle_y$ as a function of t_c, for two ratios τ_1/τ_2 corresponding to $\delta = 1.33$ and 1.8. The lines are fitted to the data. (c) The normalized oscillation frequency of the y magnetization as a function of δ. The circles show experimental results (error bars from the fits of the oscillations), while the solid line shows the prediction from Eq. (4) with no adjustable parameters. (d) The evolution of the probability $P_{\uparrow\downarrow}$ under H_{XXZ} and H_{XXX} (green shaded region), following the preparation in $|{\uparrow}{\downarrow}\rangle$. The solid lines show the simulation using the *XXZ* Hamiltonian. (b),(d) The error bars represent the standard error of the mean, which is often smaller than the symbol size.

$\delta = J_{ij}^z/J_{ij}^x = 2\tau_2/(\tau_1+\tau_2)$ is thus tunable in the range $0 < \delta < 2$. The nearest-neighbor interaction energies J_x, J_z in the engineered *XXZ* model are related to the nearest-neighbor interaction energy J by $J_x(\delta) = 2J/(2+\delta)$ and $J_z(\delta) = 2J\,\delta/(2+\delta)$.

III. EXPERIMENTAL SETUP AND PROCEDURES

Our experimental setup is based on arrays of single ^{87}Rb atoms trapped in optical tweezers [56–58]. The atoms are initialized in their ground state $|g\rangle = |5S_{1/2}, F = 2, m_F = 2\rangle$ by optical pumping (efficiency approximately 99.5%). We then switch off the tweezers, and transfer the atoms into the $|{\downarrow}\rangle = |nS_{1/2}, m_J = 1/2\rangle$ Rydberg state using a stimulated Raman adiabatic passage (STIRAP) [35] involving two lasers tuned on the $5S_{1/2}$-$6P_{3/2}$ transition at 421 nm and $6P_{3/2}$-$nS_{1/2}$ transition at 1013 nm, respectively (efficiency approximately 95%).

The microwave field couples the state $|{\downarrow}\rangle$ to a chosen Zeeman state $|{\uparrow}\rangle$ of the $nP_{3/2}$ manifold, in the presence of a 25-G magnetic field. This field is parallel to the interatomic axis for the two-atom situation and perpendicular to the plane of the atomic arrays for the remaining experiments, to ensure isotropic interactions. The microwave field at a frequency $\omega_{\text{MW}}/(2\pi)$ ranging from 5 to 10 GHz is obtained by mixing a microwave signal generated by a synthesizer with the field produced by an arbitrary waveform generator [59] operating near 200 MHz.

To initialize the system in a chosen spin state, we address specific sites within the array [60]. For this purpose, we use a spatial light modulator that imprints a specific phase pattern on a 1013 nm laser beam tuned on resonance with the $6P$-nS transition. This results in a set of focused laser beams (waist approximately 2 μm) in the atomic plane, the geometry of which corresponds to the subset of sites we wish to address, preventing the addressed atoms from interacting with the microwaves due to the Autler-Townes splitting of the nS state. We combine this addressing technique with resonant microwave rotations to excite the targeted atoms to the state $|{\uparrow}\rangle$, with the others in $|{\downarrow}\rangle$. The fidelity of this preparation is approximately 95% per atom.

Following the implementation of a particular sequence, we read out the state of the atoms. To do so, we use the 1013-nm STIRAP laser to deexcite the atoms in the $nS_{1/2}$ state to the $6P_{3/2}$ state, from which they decay back to the ground states and are recaptured in their tweezer [61]. An atom in the Rydberg state $nS_{1/2}$ is thus detected at the end of the sequence, while an atom in the $nP_{3/2}$ state is lost. This detection technique leads to false positives with a 5% probability and false negatives with 3.5% probability [62]. We include the state-preparation-and-measurement (SPAM) errors in the numerical simulations when comparing to the data.

IV. IMPLEMENTATION OF THE *XXZ* HAMILTONIAN WITH TWO ATOMS

In this section, we demonstrate the implementation of the *XXZ* Hamiltonian of Eq. (4) in the case of two interacting atoms. We use the pseudospin states $|{\downarrow}\rangle = |90S_{1/2}, m_J = 1/2\rangle$ and $|{\uparrow}\rangle = |90P_{3/2}, m_J = 3/2\rangle$ separated by $\omega_{\text{MW}}/2\pi = 5.1$ GHz and coupled by the microwave field with a mean Rabi frequency averaged over the Gaussian pulses $\Omega = 2\pi \times 7.2$ MHz. The atoms are separated by 30 μm, leading to $J \simeq 2\pi \times 930$ kHz.

The spectrum of the XXZ Hamiltonian for two atoms consists of two degenerate eigenstates $|\downarrow\downarrow\rangle$ and $|\uparrow\uparrow\rangle$ with energy J_z and two other eigenstates $|\pm\rangle = (|\uparrow\downarrow\rangle \pm |\downarrow\uparrow\rangle)/\sqrt{2}$ with energy $-J_z \pm 2J_x$. To characterize the engineering of the XXZ Hamiltonian, we first initialize the atoms in the state $|{\rightarrow}{\rightarrow}\rangle_y = (|\uparrow\uparrow\rangle - |\downarrow\downarrow\rangle + i\sqrt{2}\,|+\rangle)/2$, by applying a $\pi/2$ pulse around the x axis. We then apply one sequence of four microwave pulses, varying t_c for a fixed ratio τ_1/τ_2, i.e., a given anisotropy δ. This state evolves with time and the total y magnetization $\langle\sigma^y\rangle$ oscillates at a frequency $2|J_x - J_z|$ [see Fig. 1(b)]. We measure this frequency as a function of δ [see Fig. 1(c)] and find excellent agreement with the predicted value [see Eq. (4)].

To demonstrate the dynamical tunability of this microwave engineering, we perform an experiment in which we change the Hamiltonian during the evolution of the system. We initialize the atoms in $|\uparrow\downarrow\rangle$ and measure the probability $P_{\uparrow\downarrow}$ as a function of time. We first let the system evolve under H_{XXZ} and observe an oscillation between $|\uparrow\downarrow\rangle$ and $|\downarrow\uparrow\rangle$ at a frequency $2J$ [see Fig. 1(d)]. Between $t = 0.8 - 1.7$ μs, we apply a single microwave sequence, varying t_c while keeping $\tau_1 = \tau_2$ to engineer H_{XXX}. We observe a reduction of the oscillation frequency by a factor of 0.65(2), in agreement with the expected factor of $2/3$. We then switch off the microwaves and the exchange at frequency $2J$ resumes. This engineering does not introduce extra sizable decoherence beyond the freely evolving case. We compare the results of the experiment with the solution of the Schrödinger equation using the Hamiltonian [Eq. (4)]. We include the residual imperfections measured on the experiment: SPAM and shot-to-shot fluctuations of the interatomic distance. The results of the simulations are shown as solid lines in Fig. 1(d) and agree well with the data.

V. FREEZING OF THE MAGNETIZATION IN A 2D ARRAY

We now implement the Hamiltonian-engineering technique in a 2D square array consisting of 32 atoms (see Fig. 2). For this purpose, as has been done in Ref. [55] for a gas of cold atoms, we engineer the XXX Heisenberg model for which the total magnetization is a conserved quantity. The ability to freeze the magnetization of a system for a controllable time provides a potential route toward dynamical decoupling and quantum sensing [63].

For this experiment and for those in the next section, we use the Rydberg states $|\downarrow\rangle = |75S_{1/2}, m_J = 1/2\rangle$ and $|\uparrow\rangle = |75P_{3/2}, m_J = -1/2\rangle$, separated by $\omega_{\rm MW}/2\pi = 8.5$ GHz. We initialize the system in the $|{\rightarrow}{\rightarrow}\cdots{\rightarrow}\rangle_y$ state. We apply several sequences of the driven Hamiltonian for 3 μs and then we switch off the drive and let the system evolve under H_{XXZ}. We use $t_c = 300$ ns and Gaussian microwave pulses with a $1/e^2$ width of 16.8 ns. We measure the total magnetization $\langle\sigma^y\rangle$ after the application of an increasing number of sequences. The results are shown in Fig. 2 where, as expected, we observe an approximately constant magnetization for the first 3 μs, followed by its decay toward zero under H_{XXZ}. This demagnetization results from the beating of all the eigenfrequencies of H_{XXZ} for this many-atom system.

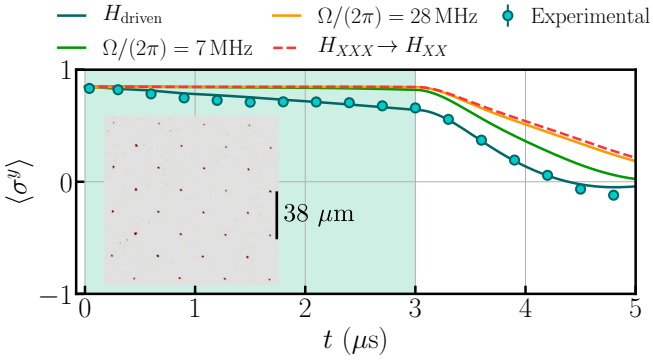

FIG. 2. The freezing of the magnetization in a 2D square array. The evolution of the total magnetization along y, $\langle\sigma^y\rangle$ after initialization in $|{\rightarrow}{\rightarrow}\cdots{\rightarrow}\rangle_y$ and evolution under $H_{\rm driven}$ for the first 3 μs and H_{XXZ} afterward. The lines show the numerical simulations based on the MACE method (see text)—all include SPAM errors: blue, $H_{\rm driven}$ including the microwave imperfections; green, without microwave imperfections; orange, pulse Rabi frequency $\Omega = 2\pi \times 28$ MHz, no microwave imperfection; dashed red, evolution under H_{XXX}, followed by H_{XXZ}. The inset shows a fluorescence image of the 2D square array containing 32 atoms with an intersite distance $a \simeq 27$ μm, leading to a nearest-neighbor interaction energy without microwaves $J \simeq 2\pi \times 133$ kHz and a mean interaction energy $J_m \simeq 2\pi \times 720$ kHz.

As the *ab initio* calculation of the dynamics is now more challenging, we use a moving-average cluster-expansion (MACE) method [64] to simulate the system. This method consists in diagonalizing clusters, here of 12 atoms, using the Schrödinger equation and averaging the results over all 12-atom cluster configurations possible with 32 atoms. We include in the simulation the SPAM errors and imperfections in the microwave pulses calibrated on a single atom (see Appendix A). As shown in Fig. 2, the simulation, without adjustable parameters, is in good agreement with the observed dynamics at all times. However, the comparison with the evolution under H_{XXZ} (red dashed line) reveals that our engineering is not perfect.

The simulation allows us to assess the contribution of various effects to explain this difference. First, not taking into account the imperfections of the microwave in the simulation (green solid line) leads to a nearly perfect freezing of the magnetization during the application of the pulses: the observed residual decay of the magnetization is thus a consequence of the microwave imperfections. Second, after switching off the microwave field, the dynamics under H_{XXZ} differ depending on whether they start from the

state produced by H_{XXX} or H_{driven} at $t = 3\ \mu$s. This difference originates from the finite duration of the microwave pulses during which the interactions play a role: an average Rabi frequency four times larger than in the experiment ($\Omega = 2\pi \times 28$ MHz, orange curve) would already lead to a nearly perfect agreement between the evolution under H_{XXX} and H_{driven}. The agreement finally indicates that the value $J_m t_c \approx 2\pi \times 0.2$ is already low enough for a faithful implementation of the *XXX* model.

VI. DYNAMICS OF DOMAIN-WALL STATES IN 1D SYSTEMS

In a last set of experiments, we illustrate the engineering of H_{XXZ} Hamiltonians on the dynamics of a domain wall (DW), i.e., a situation where a boundary separates spin-up atoms from spin-down ones, in a 1D chain with periodic (PBCs) or open (OBCs) boundary conditions. Transport properties in the nearest-neighbor *XXZ* model and for large system sizes have been studied extensively, both analytically and numerically. The evolution of such a system depends on δ due to two competing effects: a melting of the DW caused by spin flips with a rate J_x and an opposing associated energy cost of $2J_z$, which maintains the DW. In the case of a pure initial state (the relevant situation for our experiment), for $\delta < 1$, the domain wall is predicted to melt, with a magnetization profile expanding ballistically in time [65,66]. At the isotropic point ($\delta = 1$), one expects a diffusive behavior with logarithmic corrections [67]. For $\delta > 1$, the magnetization profile should be frozen at long times [42,66,68]. All these theoretical predictions have been explored for large system sizes.

Here, we study the emergence of these properties with a few-body system of ten atoms with interatomic distance $a = 19\ \mu$m [see Fig. 3(a)]. This yields a nearest-neighbor interaction $J \simeq 2\pi \times 270$ kHz and $J_m \simeq 2\pi \times 0.6$ MHz, which fulfills the condition $J_m t_c \ll 2\pi$ for $t_c = 300$ ns. Using the addressing technique described in Sec. III, we prepare five adjacent atoms in $|\uparrow\rangle$ and the remaining ones in $|\downarrow\rangle$. We then study the evolution of the system under H_{XXZ} for different δ.

We first look at the evolution of the single-site magnetization $\langle\sigma_i^z\rangle$ as a function of the normalized time $t' = t\ J_x(\delta)/(J \times 1\mu\text{s})$. The results for OBCs are shown in Fig. 3(b) with $\delta = 0, 1, 2$ [69]. For $\delta \leq 1$, we observe the melting of the domain wall, resulting in an approximately uniform magnetization profile for $t' \gtrsim 3$. In the case $\delta = 0$, the width 2ξ of the magnetization profile grows ballistically in time, as predicted, and follows a light-cone dynamics, $\xi = \pm 2J\ t'$ [65,66], illustrated by the dashed

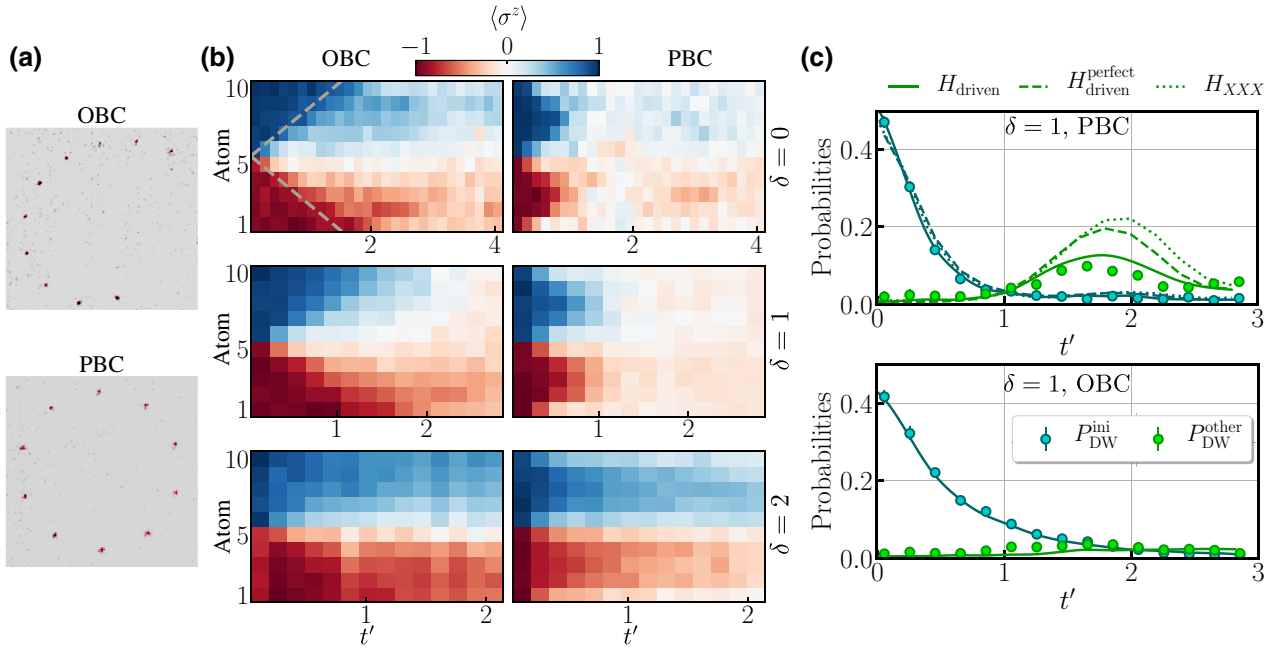

FIG. 3. The dynamics of domain-wall states under H_{XXZ} in 1D systems. (a) Fluorescence images of the trapped atoms for the two geometries used in the experiment: the spiral implements open boundary conditions (OBCs), while the circle realizes periodic boundary conditions (PBCs). (b) Density maps of the temporal evolution of the z magnetization $\langle\sigma_i^z\rangle$ as a function of the normalized time t', following the preparation of a domain-wall state, for anisotropies $\delta = 0$, 1, and 2 and OBC (left) and PBC (right) geometries. The dashed gray line shows the light cone $\xi = \pm 2Jt'$. (c) The evolution of the probability of occurrence of domain walls for OBCs and PBCs. The solid lines are the simulations using H_{driven} accounting for all experimental imperfections (SPAM errors, shot-to-shot fluctuations in atomic positions, and microwave imperfections). The dashed (dotted) line is a simulation using $H^{\text{perfect}}_{\text{driven}}$ (H_{XXZ}) without microwave imperfections.

gray lines in the top-left panel of Fig. 3(b). At the isotropic point $\delta = 1$, the melting of the wall happens more slowly, as the cost of breaking the spin domains becomes higher. For $\delta = 2$, we observe a retention of the domain wall at all times: the magnetization profile hardly evolves between $t' = 1.1$ and $t' = 2.0$, indicating a freezing of the system dynamics. Our Hamiltonian engineering is thus able to distinguish different spin-transport behaviors for various values of δ.

We now consider the case where the atoms are arranged in a circle (PBCs). One expects comparable behavior as for the OBC case, with the two domain walls melting ballistically for $\delta = 0$ and more slowly for increasing δ. This is what we observe in Fig. 3(b), with the system reaching a depolarized state more quickly than for OBCs due to the presence of two edges. However, the dynamics for $t' \gtrsim 1$ differ between PBCs and OBCs when considering as an observable the probability P_{DW} to observe a given domain wall, as we now illustrate for the case $\delta = 1$. The probability P_{DW} is defined as the probability of finding a cluster of adjacent $|\uparrow\rangle$ excitations in the chain after an evolution time. The results for the two boundary conditions are shown in Fig. 3(c) where we plot the probability $P_{\mathrm{DW}}^{\mathrm{ini}}$ of finding the *initial* domain wall after an evolution time t' [70]. We do observe the melting of the initial wall and the fact that it disappears faster for PBCs than for OBCs. We also plot the probability $P_{\mathrm{DW}}^{\mathrm{other}}$ to find a domain wall at a location *different* from the initial one. Interestingly, for PBCs, while the average magnetization reaches equilibrium [Fig. 3(b)] and the initial wall melts, $P_{\mathrm{DW}}^{\mathrm{other}}$ still evolves: domain walls appear at different locations around the circle for $t' \approx 1.7$ (see also simulations for longer times in Appendix B). The OBC case shows a much weaker transfer of the initial domain wall toward other ones, thus revealing the role of the boundary conditions.

To further understand the domain-wall structure around the circle (PBCs), we consider the spin correlations $\langle \sigma_i^z \sigma_{i+1}^z \rangle$, related to the number of spin flips N_{flip} by

$$N_{\mathrm{flip}} = \frac{1}{2} \sum_i 1 - \langle \sigma_i^z \sigma_{i+1}^z \rangle \tag{5}$$

(a flip is defined as two neighboring atoms in opposite spin states). The initialized DW state would therefore consist of two spin flips, while a fully uncorrelated state contains $N/2$ on average. We show in Fig. 4 the dynamics of N_{flip} for four values of the anisotropy for PBCs. For $\delta < 1$, N_{flip} approaches $N/2$ at long time, confirming the fact that the system becomes fully uncorrelated. However, for increasing δ, the value of N_{flip} at long times decreases. This means that the $|\uparrow\rangle$ excitations tend to remain bunched for large δ.

We finally compare the experimental data shown in Figs. 3(c) and 4 with numerical simulations using both H_{driven} and the target H_{XXZ} Hamiltonian. For both, we include SPAM errors, which are chosen to match the initial state, the residual shot-to-shot fluctuations of the interatomic distances, and the microwave imperfections for H_{driven}. The results for the simulation of the probability of domain wall are shown in Fig. 3(c): the data are well approximated by the H_{driven} simulation, indicating that we understand the sources of experimental errors. However, not including the microwave-pulse imperfections in the simulation [$H_{\mathrm{driven}}^{\mathrm{perfect}}$ in Fig. 3(c)] reveals a difference compared to the dynamics driven by H_{XXZ}. We show in Appendix B that this originates from the finite duration of the pulses during which the interaction plays a role, as observed in Sec. V. We also plot in Fig. 4 the simulation of N_{flip} using H_{driven}, including all the imperfections, and find good agreement with the data.

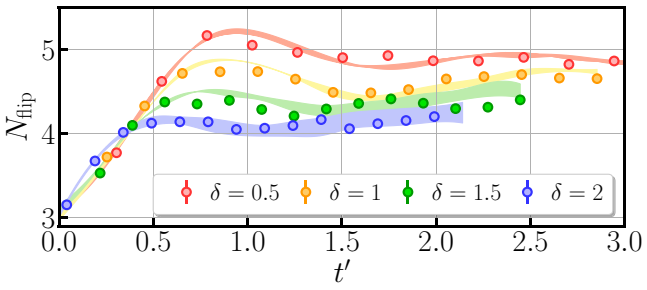

FIG. 4. The dynamics of the number of spin flips (PBCs). The evolution of N_{flip} for $\delta = 0.5$, 1, 1.5, and 2 as a function of the normalized time t'. The shaded regions show the results of the simulation using H_{driven}, including the $6 \pm 1\%$ fluctuations on the microwave rotation axis (see Appendix A).

VII. CONCLUSIONS

In this work, we engineer *XXZ* Hamiltonians with anisotropies $0 \leq \delta \leq 2$ using the resonant dipole-dipole interaction between Rydberg atoms in arrays coupled to a resonant microwave field. We illustrate the method on two iconic situations: the Heisenberg model in 2D square arrays, where we demonstrate the ability to dynamically freeze the evolution of a state with a given magnetization, and the dynamics of a domain wall in a 1D chain with open and periodic boundary conditions. By comparing our results to numerical simulations, we infer the two current limitations on our setup: (i) the imperfections in the 8.5-GHz microwave pulses and (ii) the lack of microwave power, which prevents us from reaching pulses short enough to be able to neglect the residual influence of the interactions during their application. Despite these limitations, which can be solved by improving the microwave hardware, we are able to observe all the qualitative features of the situations that we explore. This highlights the versatility of a Rydberg-based quantum simulator, beyond the

implementation of the natural Ising-like or *XXZ* Hamiltonians. Future work could include the study of frustration in various arrays governed by the Heisenberg model [71] or the study of domain-wall dynamics for larger system sizes to confirm the various delocalization scalings beyond the emergent behaviors studied here. We also anticipate that combination of the microwave drive with the ability to locally address the resonance frequency of the atoms using light shifts would lead to the engineering of a broader class of Hamiltonians.

ACKNOWLEDGMENTS

This work is supported by the European Union (EU) Horizon 2020 research and innovation program "Programmable Atomic Large-Scale Quantum Simulation" (PASQuanS) under Grant Agreement No. 817482, the Agence National de la Recherche (ANR, project RYBOTIN), the Deutsche Forschungsgemeinschaft (DFG, German Research Foundation) under Germany's Excellence Strategy EXC2181/1-390900948 (the Heidelberg STRUCTURES Excellence Cluster), within the Collaborative Research Center SFB1225 (ISOQUANT), the DFG Priority Program 1929 "GiRyd" (DFG WE2661/12-1), and by the Heidelberg Center for Quantum Dynamics. C.H. acknowledges funding from the Alexander von Humboldt foundation, T.F. from a graduate scholarship of the Heidelberg University (LGFG), and D.B. from the Ramón y Cajal program (RYC2018-025348-I). F.W. is partially supported by the Erasmus+ program of the EU. We also acknowledge support by the state of Baden-Württemberg through Baden-Württemberg high performance computing (bwHPC) and the DFG through Grant No. INST 40/575-1 FUGG (JUSTUS 2 cluster).

APPENDIX A: CALIBRATION OF THE MICROWAVE-PULSE SEQUENCE ON A SINGLE ATOM

The microwave field is sent onto the atoms using a microwave antenna, with poor control over the polarization due to the presence of metallic parts surrounding the atoms. An example of Rabi oscillation on the $|\downarrow\rangle - |\uparrow\rangle$ transition using a long microwave pulse is shown in Fig. 5(a). We observe no appreciable damping after 25 oscillations.

To implement H_{driven}, we find empirically that the application of pulses with Gaussian, rather than square, envelopes minimizes pulse errors arising from the fast on-off switching. In order to assess the influence of further imperfections in the microwave pulses on the dynamics of the systems used in this work, we compare *single*-atom data with a numerical simulation. We prepare an atom in $|\downarrow\rangle = |75S_{1/2}, m_J = 1/2\rangle$ and then implement sequences of four $\pi/2$ Gaussian pulses, in the same way as for the many-body system. Following a single four-pulse

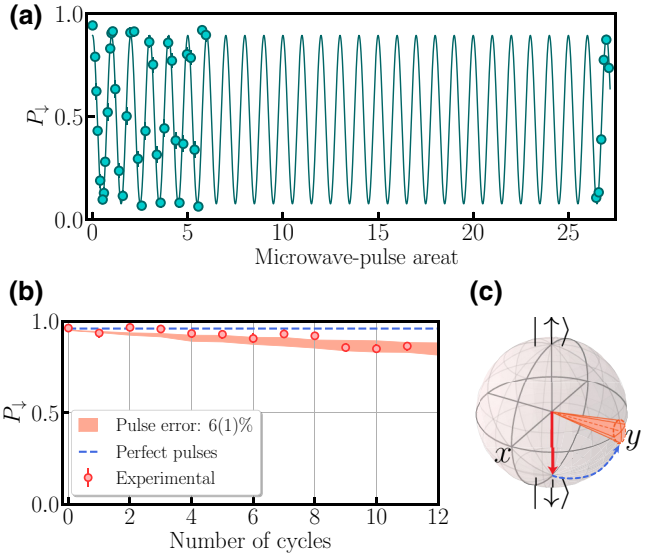

FIG. 5. The calibration of microwave-pulse error. (a) Microwave Rabi oscillations between states $|\uparrow\rangle$ and $|\downarrow\rangle$. The Rabi frequency is $\Omega = 2\pi \times 13.2$ MHz. (b) The probability $P_\downarrow$ of measuring a single atom in $|\downarrow\rangle$ following H_{XXX} versus the number of cycles. The data are shown as red circles, with the simulated pulse sequence results for perfect pulses shown in blue and with a pulse error $\Delta\theta = 0.06 \pm 0.01$ as the shaded pink region. (c) An illustration of how the error is included in the simulation: the final Bloch vector after a rotation around any axis (here, the x axis) lies inside the orange cone.

cycle, one would expect the atom to have returned to $|\downarrow\rangle$. Figure 5(b) shows the probability of measuring the atom in $|\downarrow\rangle$ after each cycle, where we see a slow decrease in $P_\downarrow$.

In the main text, we conclude that part of the discrepancy between the experimental results and the prediction of the *XXZ* Hamiltonian simulation comes from errors in the microwave pulses. The source of these errors could be fluctuations in the amplitude and/or the phase of the microwave pulses, which are difficult to measure at frequencies in the (5–10)-GHz range. To encompass these effects, we phenomenologically include in our simulations an uncertainty in the angle of rotation of the microwave pulse: for each pulse, we assign two values n_1 and n_2 from a normal distribution centered around zero with a standard deviation $\Delta\theta$. We then use these values to describe the rotation operator: if the desired rotation axis is x, the actual rotation is performed around the x' axis such that

$$\sigma^{x'} = (1 - n_1^2 - n_2^2)^{1/2}\sigma^x + n_1\sigma^y + n_2\sigma^z. \tag{A1}$$

This effect is illustrated in Fig. 5(c). In Fig. 5(b), the shaded area shows an uncertainty in pulse error of $\Delta\theta = 0.06 \pm 0.01$, which closely matches the experimental results. We use this value of the uncertainty in all the many-body simulations using H_{driven} presented in this work.

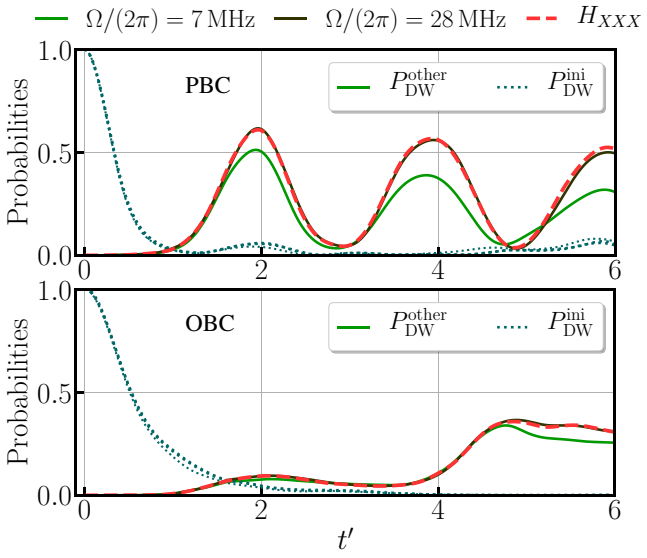

FIG. 6. The influence of the finite duration of the microwave pulses. A comparison between the evolution of the probabilities of domain walls under H_{driven} and H_{XXX} in PBCs (upper) and OBCs (lower). The simulations do not include any experimental error to highlight the role of the finite duration of the microwave pulses, with average Rabi frequency Ω. The large increase of P_{DW} observed for $t' > 4$ in OBCs is a consequence of the reflection of the excitations at the edges of the chain.

APPENDIX B: INFLUENCE OF THE FINITE DURATION OF THE MICROWAVE PULSES ON THE SIMULATED MANY-BODY HAMILTONIAN

We see in Sec. V that, in the case of the 2D array, increasing the Rabi frequency of the microwave pulses by a factor of 4, i.e., decreasing their duration by a factor of 4, leads to a nearly perfect agreement between the evolution under H_{driven} and H_{XXX}. Here, we perform the same analysis for the evolution of the domain wall for both PBCs and OBCs (Sec. VI). The results of the simulation of the probability of a domain wall *without* experimental imperfections is shown in Fig. 6 for an evolution longer than that achieved in the experiment and for two Rabi frequencies. Similarly to the 2D case, a Rabi frequency four times as large as the one we can reach in the experiment would lead to a very good agreement with the evolution under H_{XXX}. This simulation here also indicates that the value $J_m t_c \approx 2\pi \times 0.2$ is low enough and that the use of discrete pulses does not thwart a faithful implementation of the *XXZ* Hamiltonian.

[1] I. M. Georgescu, S. Ashhab, and F. Nori, Quantum simulation, Rev. Mod. Phys. **86**, 153 (2014).

[2] R. Blatt and C. F. Roos, Quantum simulations with trapped ions, Nat. Phys. **8**, 277 (2012).

[3] C. Monroe, W. C. Campbell, L.-M. Duan, Z.-X. Gong, A. V. Gorshkov, P. W. Hess, R. Islam, K. Kim, N. M. Linke, G. Pagano, P. Richerme, C. Senko, and N. Y. Yao, Programmable quantum simulations of spin systems with trapped ions, Rev. Mod. Phys. **93**, 025001 (2021).

[4] Y. L. Zhou, M. Ortner, and P. Rabl, Long-range and frustrated spin-spin interactions in crystals of cold polar molecules, Phys. Rev. A **84**, 052332 (2011).

[5] B. Yan, S. A. Moses, B. Gadway, J. P. Covey, K. R. A. Hazzard, A. M. Rey, D. S. Jin, and J. Ye, Observation of dipolar spin-exchange interactions with lattice-confined polar molecules, Nature **501**, 521 (2013).

[6] I. Bloch, J. Dalibard, and S. Nascimbène, Quantum simulations with ultracold quantum gases, Nat. Phys. **8**, 267 (2012).

[7] C. Gross and I. Bloch, Quantum simulations with ultracold atoms in optical lattices, Science **357**, 995 (2017).

[8] A. A. Houck, H. E. Türeci, and J. Koch, On-chip quantum simulation with superconducting circuits, Nat. Phys. **8**, 292 (2012).

[9] M. Kjaergaard, M. E. Schwartz, J. Braumüller, P. Krantz, J. I.-J. Wang, S. Gustavsson, and W. D. Oliver, Superconducting qubits: Current state of play, Annu. Rev. Condens. Matter Phys. **11**, 369 (2020).

[10] N. Goldman and J. Dalibard, Periodically Driven Quantum Systems: Effective Hamiltonians and Engineered Gauge Fields, Phys. Rev. X **4**, 031027 (2014).

[11] J. H. Shirley, Solution of the Schrödinger equation with a Hamiltonian periodic in time, Phys. Rev. **138**, B979 (1965).

[12] L. M. K. Vandersypen and I. L. Chuang, NMR techniques for quantum control and computation, Rev. Mod. Phys. **76**, 1037 (2005).

[13] Y. Salathé, M. Mondal, M. Oppliger, J. Heinsoo, P. Kurpiers, A. Potočnik, A. Mezzacapo, U. Las Heras, L. Lamata, E. Solano, S. Filipp, and A. Wallraff, Digital Quantum Simulation of Spin Models with Circuit Quantum Electrodynamics, Phys. Rev. X **5**, 021027 (2015).

[14] P. Jurcevic, H. Shen, P. Hauke, C. Maier, T. Brydges, C. Hempel, B. P. Lanyon, M. Heyl, R. Blatt, and C. F. Roos, Direct Observation of Dynamical Quantum Phase Transitions in an Interacting Many-Body System, Phys. Rev. Lett. **119**, 080501 (2017).

[15] P. Peng, C. Yin, X. Huang, C. Ramanathan, and P. Cappellaro, Floquet prethermalization in dipolar spin chains, Nat. Phys. **17**, 444 (2021).

[16] A. Rubio-Abadal, M. Ippoliti, S. Hollerith, D. Wei, J. Rui, S. L. Sondhi, V. Khemani, C. Gross, and I. Bloch, Floquet Prethermalization in a Bose-Hubbard System, Phys. Rev. X **10**, 021044 (2020).

[17] A. Kyprianidis, F. Machado, W. Morong, P. Becker, K. S. Collins, D. V. Else, L. Feng, P. W. Hess, C. Nayak, G. Pagano, N. Y. Yao, and C. Monroe, Observation of a prethermal discrete time crystal, Science **372**, 1192 (2021).

[18] M. Aidelsburger, M. Atala, M. Lohse, J. T. Barreiro, B. Paredes, and I. Bloch, Realization of the Hofstadter Hamiltonian with Ultracold Atoms in Optical Lattices, Phys. Rev. Lett. **111**, 185301 (2013).

[19] N. Fläschner, B. S. Rem, M. Tarnowski, D. Vogel, D.-S. Lühmann, K. Sengstock, and C. Weitenberg, Experimental reconstruction of the Berry curvature in a Floquet Bloch band, Science **352**, 1091 (2016).

[20] F. Meinert, M. J. Mark, K. Lauber, A. J. Daley, and H.-C. Nägerl, Floquet Engineering of Correlated Tunneling in the Bose-Hubbard Model with Ultracold Atoms, Phys. Rev. Lett. **116**, 205301 (2016).

[21] C. Schweizer, F. Grusdt, M. Berngruber, L. Barbiero, E. Demler, N. Goldman, I. Bloch, and M. Aidelsburger, Floquet approach to Z_2 lattice gauge theories with ultracold atoms in optical lattices, Nat. Phys. **15**, 1168 (2019).

[22] A. Eckardt, Colloquium: Atomic quantum gases in periodically driven optical lattices, Rev. Mod. Phys. **89**, 011004 (2017).

[23] K. Wintersperger, C. Braun, F. N. Ünal, A. Eckardt, M. D. Liberto, N. Goldman, I. Bloch, and M. Aidelsburger, Realization of an anomalous Floquet topological system with ultracold atoms, Nat. Phys. **16**, 1058 (2020).

[24] A. Browaeys and T. Lahaye, Many-body physics with individually controlled Rydberg atoms, Nat. Phys. **16**, 132 (2020).

[25] L. Henriet, L. Beguin, A. Signoles, T. Lahaye, A. Browaeys, G.-O. Reymond, and C. Jurczak, Quantum computing with neutral atoms, Quantum **4**, 327 (2020).

[26] M. Morgado and S. Whitlock, Quantum simulation and computing with Rydberg-interacting qubits, AVS Quantum Sci. **3**, 023501 (2021).

[27] E. Guardado-Sanchez, P. T. Brown, D. Mitra, T. Devakul, D. A. Huse, P. Schauß, and W. S. Bakr, Probing the Quench Dynamics of Antiferromagnetic Correlations in a 2D Quantum Ising Spin System, Phys. Rev. X **8**, 021069 (2018).

[28] V. Lienhard, S. de Léséleuc, D. Barredo, T. Lahaye, A. Browaeys, M. Schuler, L.-P. Henry, and A. M. Läuchli, Observing the Space- and Time-Dependent Growth of Correlations in Dynamically Tuned Synthetic Ising Antiferromagnets, Phys. Rev. X **8**, 021070 (2018).

[29] P. Scholl, M. Schuler, H. J. Williams, A. A. Eberharter, D. Barredo, K.-N. Schymik, V. Lienhard, L.-P. Henry, T. C. Lang, T. Lahaye, A. M. Läuchli, and A. Browaeys, Quantum simulation of 2D antiferromagnets with hundreds of Rydberg atoms, Nature **595**, 233 (2021).

[30] Y. Song, M. Kim, H. Hwang, W. Lee, and J. Ahn, Quantum simulation of Cayley-tree Ising Hamiltonians with three-dimensional Rydberg atoms, Phys. Rev. Res. **3**, 013286 (2021).

[31] A. Keesling, A. Omran, H. Levine, H. Bernien, H. Pichler, S. Choi, R. Samajdar, S. Schwartz, P. Silvi, S. Sachdev, P. Zoller, M. Endres, M. Greiner, V. Vuletic, and M. D. Lukin, Quantum Kibble-Zurek mechanism and critical dynamics on a programmable Rydberg simulator, Nature **568**, 207 (2019).

[32] S. Ebadi, T. T. Wang, H. Levine, A. Keesling, G. Semeghini, A. Omran, D. Bluvstein, R. Samajdar, H. Pichler, W. W. Ho, S. Choi, S. Sachdev, M. Greiner, V. Vuletić, and M. D. Lukin, Quantum phases of matter on a 256-atom programmable quantum simulator, Nature **595**, 227 (2021).

[33] G. Semeghini, H. Levine, A. Keesling, S. Ebadi, T. T. Wang, D. Bluvstein, R. Verresen, H. Pichler, M. Kalinowski, R. Samajdar, A. Omran, S. Sachdev, A. Vishwanath, M. Greiner, V. Vuletić, and M. D. Lukin, Probing topological spin liquids on a programmable quantum simulator, Science **374**, 1242 (2021).

[34] V. Lienhard, P. Scholl, S. Weber, D. Barredo, S. de Léséleuc, R. Bai, N. Lang, M. Fleischhauer, H. P. Büchler, T. Lahaye, and A. Browaeys, Realization of a Density-Dependent Peierls Phase in a Synthetic, Spin-Orbit Coupled Rydberg System, Phys. Rev. X **10**, 021031 (2020).

[35] S. de Léséleuc, V. Lienhard, P. Scholl, D. Barredo, S. Weber, N. Lang, H. P. Büchler, T. Lahaye, and A. Browaeys, Observation of a symmetry-protected topological phase of interacting bosons with Rydberg atoms, Science **365**, 775 (2019).

[36] S. Whitlock, A. W. Glaetzle, and P. Hannaford, Simulating quantum spin models using Rydberg-excited atomic ensembles in magnetic microtrap arrays, J. Phys. B: At., Mol. Opt. Phys. **50**, 074001 (2017).

[37] A. Signoles, T. Franz, R. Ferracini Alves, M. Gärttner, S. Whitlock, G. Zürn, and M. Weidemüller, Glassy Dynamics in a Disordered Heisenberg Quantum Spin System, Phys. Rev. X **11**, 011011 (2021).

[38] T. L. Nguyen, J. M. Raimond, C. Sayrin, R. Cortiñas, T. Cantat-Moltrecht, F. Assemat, I. Dotsenko, S. Gleyzes, S. Haroche, G. Roux, T. Jolicoeur, and M. Brune, Towards Quantum Simulation with Circular Rydberg Atoms, Phys. Rev. X **8**, 011032 (2018).

[39] D. V. Dmitriev, V. Y. Krivnov, A. A. Ovchinnikov, and A. Langari, One-dimensional anisotropic Heisenberg model in the transverse magnetic field, J. Exp. Theor. Phys. **95**, 538 (2002).

[40] K. X. Wei, C. Ramanathan, and P. Cappellaro, Exploring Localization in Nuclear Spin Chains, Phys. Rev. Lett. **120**, 070501 (2018).

[41] M. Cheneau, P. Barmettler, D. Poletti, M. Endres, P. Schauß, T. Fukuhara, C. Gross, I. Bloch, C. Kollath, and S. Kuhr, Light-cone-like spreading of correlations in a quantum many-body system, Nature **481**, 484 (2012).

[42] D. Gobert, C. Kollath, U. Schollwöck, and G. Schütz, Real-time dynamics in spin-1/2 chains with adaptive time-dependent density matrix renormalization group, Phys. Rev. E **71**, 036102 (2005).

[43] J. Sirker, R. G. Pereira, and I. Affleck, Diffusion and Ballistic Transport in One-Dimensional Quantum Systems, Phys. Rev. Lett. **103**, 216602 (2009).

[44] P. Barmettler, M. Punk, V. Gritsev, E. Demler, and E. Altman, Relaxation of Antiferromagnetic Order in Spin-1/2 Chains Following a Quantum Quench, Phys. Rev. Lett. **102**, 130603 (2009).

[45] B. Bertini, F. Heidrich-Meisner, C. Karrasch, T. Prosen, R. Steinigeweg, and M. Žnidarič, Finite-temperature transport in one-dimensional quantum lattice models, Rev. Mod. Phys. **93**, 025003 (2021).

[46] T. Giamarchi, *Quantum Physics in One Dimension* (Clarendon Press, Oxford, 2003).

[47] P. N. Jepsen, J. Amato-Grill, I. Dimitrova, W. W. Ho, E. Demler, and W. Ketterle, Spin transport in a tunable Heisenberg model realized with ultracold atoms, Nature **588**, 403 (2020).

[48] S. Hild, T. Fukuhara, P. Schauß, J. Zeiher, M. Knap, E. Demler, I. Bloch, and C. Gross, Far-from-Equilibrium Spin Transport in Heisenberg Quantum Magnets, Phys. Rev. Lett. **113**, 147205 (2014).

[49] D. Wei, A. Rubio-Abadal, B. Ye, F. Machado, J. Kemp, K. Srakaew, S. Hollerith, J. Rui, S. Gopalakrishnan,

N. Y. Yao, I. Bloch, and J. Zeiher, Quantum gas microscopy of Kardar-Parisi-Zhang superdiffusion (2021), ArXiv:2107.00038.

[50] M. K. Joshi, F. Kranzl, A. Schuckert, I. Lovas, C. Maier, R. Blatt, M. Knap, and C. F. Roos, Observing emergent hydrodynamics in a long-range quantum magnet (2021), ArXiv:2107.00033.

[51] P. Richerme, Z.-X. Gong, A. Lee, C. Senko, J. Smith, M. Foss-Feig, S. Michalakis, A. V. Gorshkov, and C. Monroe, Non-local propagation of correlations in quantum systems with long-range interactions, Nature **511**, 198 (2014).

[52] P. Jurcevic, B. P. Lanyon, P. Hauke, C. Hempel, P. Zoller, R. Blatt, and C. F. Roos, Quasiparticle engineering and entanglement propagation in a quantum many-body system, Nature **511**, 202 (2014).

[53] W. L. Tan, P. Becker, F. Liu, G. Pagano, K. S. Collins, A. De, L. Feng, H. B. Kaplan, A. Kyprianidis, R. Lundgren, W. Morong, S. Whitsitt, A. V. Gorshkov, and C. Monroe, Domain-wall confinement and dynamics in a quantum simulator, Nat. Phys. **17**, 742 (2021).

[54] T. Fukuhara, P. Schauß, M. Endres, S. Hild, M. Cheneau, I. Bloch, and C. Gross, Microscopic observation of magnon bound states and their dynamics, Nature **502**, 76 (2013).

[55] S. Geier, N. Thaicharoen, C. Hainaut, T. Franz, A. Salzinger, A. Tebben, D. Grimshandl, G. Zürn, and M. Weidemüller, Floquet Hamiltonian engineering of an isolated many-body spin system, Science **374**, 1149 (2021).

[56] D. Barredo, V. Lienhard, S. de Léséleuc, T. Lahaye, and A. Browaeys, Synthetic three-dimensional atomic structures assembled atom by atom, Nature **561**, 79 (2018).

[57] F. Nogrette, H. Labuhn, S. Ravets, D. Barredo, L. Béguin, A. Vernier, T. Lahaye, and A. Browaeys, Single-Atom Trapping in Holographic 2D Arrays of Microtraps with Arbitrary Geometries, Phys. Rev. X **4**, 021034 (2014).

[58] K.-N. Schymik, V. Lienhard, D. Barredo, P. Scholl, H. Williams, A. Browaeys, and T. Lahaye, Enhanced atom-by-atom assembly of arbitrary tweezer arrays, Phys. Rev. A **102**, 063107 (2020).

[59] Tabor Electronics Ltd. SE5081.

[60] S. de Léséleuc, D. Barredo, V. Lienhard, A. Browaeys, and T. Lahaye, Optical Control of the Resonant Dipole-Dipole Interaction between Rydberg Atoms, Phys. Rev. Lett. **119**, 053202 (2017).

[61] For the experiments beyond two atoms, prior to sending the 1013-nm deexcitation laser, we first apply a microwave pulse of 30ns to transfer atoms in $|\uparrow\rangle$ to $|75D_{3/2}, m_J = -3/2\rangle$, which has a much smaller coupling to $|\downarrow\rangle$. This procedure leads to a freezing of the interaction-induced dynamics.

[62] S. de Léséleuc, D. Barredo, V. Lienhard, A. Browaeys, and T. Lahaye, Analysis of imperfections in the coherent optical excitation of single atoms to Rydberg states, Phys. Rev. A **97**, 053803 (2018).

[63] J. Choi, H. Zhou, H. S. Knowles, R. Landig, S. Choi, and M. D. Lukin, Robust Dynamic Hamiltonian Engineering of Many-Body Spin Systems, Phys. Rev. X **10**, 031002 (2020).

[64] K. R. A. Hazzard, B. Gadway, M. Foss-Feig, B. Yan, S. A. Moses, J. P. Covey, N. Y. Yao, M. D. Lukin, J. Ye, D. S. Jin, and A. M. Rey, Many-Body Dynamics of Dipolar Molecules in an Optical Lattice, Phys. Rev. Lett. **113**, 195302 (2014).

[65] M. Collura, A. De Luca, and J. Viti, Analytic solution of the domain-wall nonequilibrium stationary state, Phys. Rev. B **97**, 081111 (2018).

[66] G. Misguich, N. Pavloff, and V. Pasquier, Domain wall problem in the quantum *XXZ* chain and semiclassical behavior close to the isotropic point, SciPost Phys. **7**, eid 025 (2019).

[67] G. Misguich, K. Mallick, and P. L. Krapivsky, Dynamics of the spin-1/2 Heisenberg chain initialized in a domain-wall state, Phys. Rev. B **96**, 195151 (2017).

[68] J. Mossel and J.-S. Caux, Relaxation dynamics in the gapped *XXZ* spin-1/2 chain, New J. Phys. **12**, 055028 (2010).

[69] The implementation of $H_X XZ2X$ requires $\tau_1 = 0$. We therefore remove the X and $-X$ pulses from the sequence, with the exception of the first and final pulses.

[70] To increase the amplitude of the revival in $P_D W^{\text{other}}$ observed in Fig. 3(c), we include in the data and in the simulations events containing domain walls with four, five, and six excitations.

[71] J. Richter, J. Schulenburg, and A. Honecker, in *Quantum magnetism. Lecture Notes in Physics*, edited by U. Schollwöck, J. Richter, D. Farnell, and R. Bishop (Springer, Berlin, 2004), p. 85.